J Mater Sci (2011) 46:2548–2556
DOI 10.1007/s10853-010-5107-y

Evaluation of defects in materials using resonant ultrasound spectroscopy

Kevin Flynn · Miladin Radovic

Received: 15 June 2010 / Accepted: 22 November 2010 / Published online: 23 December 2010

Abstract This study demonstrates the practicability of using Resonant Ultrasound Spectroscopy (RUS) in combination with Finite Element Analysis (FEA) as a non-destructive technique for determining the size and location of defects in axisymmetrical samples of known geometry, mass, and elastic constants. Experiments and calculations were conducted on steel samples with thin cuts of different lengths and locations. Frequency spectra measured by RUS were found to match closely the frequency spectra calculated by FEM for the steel specimens before and after the introduction of the thin cut. Analyses of the series of FEM-generated frequency spectra showed some patterns in resonant frequency shifts as a function of the size and location of the thin cut. Therefore, based on the analysis of sufficient number of FEA models, it was possible to develop a methodology for determining sizes and locations of defects in examined objects from the resonant frequencies measured by RUS with a high accuracy that does not exceed 2% for the length of defects and 5% for their location.

Introduction

Non-destructive Testing (NDT) methods have been used for centuries to test the quality of different products without damaging them. A large number of different methods and techniques have been developed [1–3] to detect defects in different components, including dye-penetrate, radiographic, impulse excitation, ultrasonic, electromagnetic, acoustic emission, thermograph, etc. One of the oldest group of NDT methods, namely resonant methods, are based on resonant response of the particular component. For example, wheel-tappers tap the wheels of locomotives and listen to the sound they produce to detect the presence of cracks, while ordinary customers can usually be seen in shops around the globe tapping glass objects to check for the presence of defects before making a purchase. However, over the last few decades, resonant NDT has grown far beyond tapping glasses or locomotive wheels.

Among many different types of NDT techniques, resonant techniques are particularly interesting because they allow for easy and inexpensive detection of both internal and surface defects with a single test. Resonant NDT techniques are based on identifying one or more natural resonant frequencies [2, 4] that are functions of geometry, mass, and elastic constants (stiffness) of examined object. Resonant (or natural) frequencies of a system can be either measured or calculated by solving equations of motion for the known shape [5]. The reverse is also true; if resonant frequencies of an object are known, its elastic properties can be determined [4, 6, 7]. Since natural frequencies of an object depend on its elastic constants, mass, and geometry of the system, any defect may be expected to produce changes in the resonant frequency spectrum [8–10]. In other words, the foundation of resonant NDT methods lies on the possibility to identify defective objects by analyzing their resonant frequencies.

Impact excitation is the simplest resonant non-destructive technique that identifies the natural frequency of a test component by applying a brief impact and measuring the frequency of the resulting vibration of the object [11–13]. A comparison of the measured frequency to the predicted or calculated resonant frequency of the undamaged component of the same geometry and size shows if the test object is defective [12, 13]. Advantages of impact testing

K. Flynn · M. Radovic (✉)
Department of Mechanical Engineering, Texas A&M University, College Station, TX 77843-3123, USA
e-mail: mradovic@tamu.edu

include ease of application, possibility of detecting a defect in the entire component, not only on its surface, and its applicability to almost any geometry for which non-defective resonant frequency data can be acquired [11, 14]. Main disadvantages are the extensive analysis (either computational or experimental) that is required to determine acceptability criteria, uncontrolled excitation force, and the sensitivity of the results to any change in dimensions or any other physical characteristics of the test object [9–11]. In other words, resonant frequencies of a test object are affected by many factors, any one of which might produce results that appear unacceptable [12].

Relatively recently, Resonant Ultrasound Spectroscopy (RUS) was proposed as a NDT for identifying and evaluating defects. RUS has been mostly used as one of the most accurate techniques for measuring the elastic moduli of different solids since the 1960s [4, 15]. In recent years, RUS has received increasing attention due to its potential for quality control applications [4, 7, 16]. Briefly, RUS NDT is based on measuring a large number of free-body mode resonant frequencies—a frequency spectrum—of an examined object [4, 6, 7, 16–19]. When an outside oscillatory force is applied to an object, the object will have a larger response (amplitude) if that force oscillates at the frequency that is equal to one or more of the system's resonant frequencies [5, 20]. Using this principle it is possible to determine resonant frequencies by identifying the amplitude peak responses of an object that is forced to vibrate at various frequencies [4].

All resonant frequencies within a frequency spectrum will be affected by the eventual presence of a defect. However, some frequencies will be affected more than others depending on the location of the defect. For example, a longitudinal crack in a solid cylinder would probably have a greater effect on the frequency that corresponds to the longitudinal bending and torsional modes than to the transverse bending mode [4]. Therefore, a comparison of the spectrum of an undamaged object to that of an examined one can be used to determine if the examined object is damaged and, possibly, to identify the location and severity of the defect [4, 8, 11].

Defects in an object may be identified from a resonant frequency spectrum by resonant frequency shifts, peak splitting, increases in peak width, and changes in amplitude [4].

- *Resonance frequency shift* is the most common way of indentifying the presence of defects in examined objects since damages change the physical properties of an object, and thus the resonant frequencies [4]. For example, cracks tend to reduce resonant frequencies although the magnitude of frequency shift is not the same for all vibration modes [4].
- *Peak splitting* is a second method that can be used to identify defects within an object with rotational symmetry [19]. For example, some of the resonant frequencies for objects with 90° rotational symmetry fall on the exact same value [4, 5, 10, 19, 21]. Typically, defects eliminate the axial symmetry and result in peak splitting since overlapping resonant frequencies of two different modes shift for different amounts [4].
- *Increases in peak width* may also indicate the presence of defects [17]. An increase in internal damping due to presence of defects causes widening of the resonant peaks in RUS spectra [17]. This is particularly useful for defect detection when the crack is very small or in the case of wet/dry testing [4, 17].
- *Changes in response amplitude* at a particular frequency can also be used to identify the presence of defects [4]. However, to determine changes in the response amplitude, the excitation force must be the same in all cases, and the response of the object must be measured at the same point, which is not easy to achieve in practice.

If one or more resonant frequencies of an examined object are outside the acceptable range, the tested object is assumed to be flawed [4, 7]. An acceptable range of frequency spectra is usually determined by performing RUS tests on a large number of identical objects which are known to be acceptable. It is obvious that one of the major advantages of RUS over the most other NDT techniques is its capability to test the entire object simultaneously to identify the presence of defects [4]. Any defect, no matter where located, will affect one or more resonance frequencies in the frequency spectrum of the object. In addition, testing and analysis processes can be easily automated and integrated in a production process [4]. However, an obvious disadvantage of this method is the requirement for testing many parts of known quality to determine the acceptability criteria.

Here, we explore the possibility of determining acceptability criteria for RUS NDT without testing a large number of undamaged and damaged objects. Free-body mode resonant frequencies of an object with and without a large number of various defects can be determined using a finite element modeling (FEM) analysis. The FEM analysis can be further used to develop acceptability criteria for the particular object. In addition, it is possible not only to detect the presence of defects using this method but also to determine some of the characteristics of the defects (such as location and size) by analyzing a series of FEM-generated frequency spectrum.

The idea of using RUS in combination with FEM to analyze defects in components goes back to 70s when first

attempts were made to identify the location of defects by using resonant frequencies calculated from FEM models [14]. FEM has been successfully used to identify resonant frequencies of undamaged objects with different geometries [4, 8–10, 14, 17, 18, 22]. Lee et al. [9], Kam et al. [8], and Rizos et al. [10] used FEM-generated resonance frequencies to identify the location and depth of a defect in a one-dimensional beam model. However, some of these early efforts did not test the accuracy of FEM predictions by comparing them with experimentally generated resonant spectra of the actual defective parts. In addition, all those models were developed for relatively large defects [8–10, 14]. Recently, Belyaev et al. [17] attempted to use RUS to determine crack depths in silicon wafers. They found that FEM predictions of resonant frequencies for undamaged specimens were within acceptable limits when compared to the actual experiential results and that FEM-predicted mode shapes closely matched actual mode shapes [18]. However, they found a substantial variation between actual and predicted resonant frequencies for silicon wafers with defects. They suggested that the reason for observed discrepancies between FEM predictions and experimental results lies in the physical interaction between crack surfaces in the real objects [17].

Experimental and numerical methods

In this study, the RUSpec (Magnaflux Quasar Systems, NM) resonant spectrometer, together with Galaxy software (Magnaflux Quasar Systems, NM), was used to collect resonant spectra of examined samples. Small parallelepiped samples were rested lightly on three piezoelectric transducers. The frequency of the driving transducer was swept through a range of frequencies of interest, which corresponded to one or more of the resonant frequencies of the sample. The other two transducers were used to measure the response of the sample [4, 7, 16].

Galaxy RPModel v2.68b (Magnaflux Quasar Systems, NM) software was used to determine resonant frequencies of the examined undamaged samples in the shape of parallelepipeds. This software calculates resonant frequencies of objects by minimization of Lagrangian equations for free-body vibrations using the Rayleigh–Ritz method [4, 22]. The same software was also used to determine elastic constants of a material. However, measured resonant spectrum cannot be deconvoluted directly to deduce the elastic constants of the specimens. Instead, an approximate spectrum was calculated from the known sample dimensions, density, and a set of "guessed" elastic constants. A multidimensional Levenberg–Marquardt algorithm was further used to determine elastic constants of the solid from a single frequency scan through an iterative process of minimization of the root-mean-square (RMS) error between measured and calculated resonant peaks [4, 22, 23]. Elastic constants determined from RUS spectra were further used to calculate resonance peaks of examined samples with and without defects.

Solving equations of motion to determine resonant frequencies of objects numerically becomes very complex when applied to real systems, especially objects with defects, while another method based on minimization of Lagrange's equation is only applicable to geometries that can be approximated by continuous functions [20]. However, Finite Element Analysis (FEA) provides a simple way of determining natural resonant frequencies of an object with a complex geometry. FEA solves the problems of complex geometries by reducing any object to a large number of simple building blocks. Then, it is possible to approximate equations of motion for each block and to solve them numerically and simultaneously using different codes [24–26]. In this work, Dassault Systems SolidWorks Education Edition SP4.0 2007 and CosmosWorks SP3.1 2004 were used to determine resonant frequencies numerically for examined samples with and without defects.

Examined specimens were standard 4140 steel $12.6 \times 12.6 \times 26.2$ mm^3 bars with cut notches, Fig. 1. Cuts of different lengths were made partway through each specimen at different locations, as it is shown in Fig. 1 and Table 1. A 0.75 mm thick diamond blade produced a cut approximately 1.0 mm in width. Dimensions of the notches were measured using an optical microscope. Resonant spectra of the specimens were collected by RUS before and after cutting the notches. In Table 1, the *X*, *Y*, and *Z* dimensions correspond to the length, width, and height of

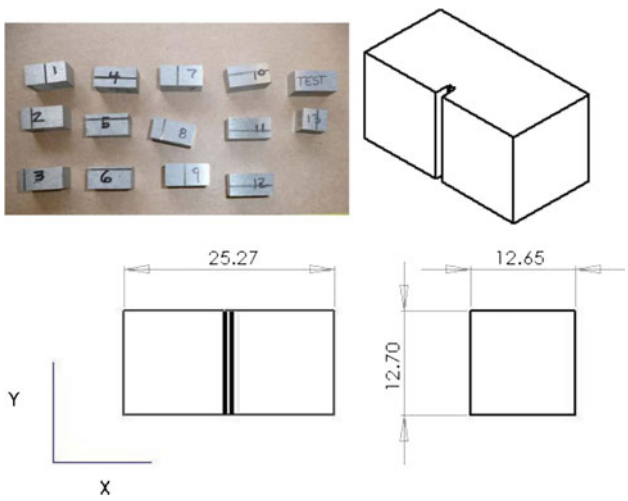

Fig. 1 Schematic of samples showing direction of *X* and *Y* axes (*Z* is out-of-plane). All dimensions are in millimeters. *Inserted photo* shows specimens with different positions of notches

Table 1 Dimensions, mass, and position of notches for examined samples

Dimensions				Elastic constants			Cut location				
Samples (nm)	*X*	*Y*	*Z*	Initial weight (g)	C_{11} (GPa)	C_{44} (GPa)	Plane	Axis	Distance from axis (mm)	Depth (mm)	Width (mm)
1	25.27	12.68	12.65	31.96	273.6	83.0	*Y–Z*	*Y*	12.60	2.35	1.05
2	25.25	12.68	12.66	31.92	273.7	82.9	*Y–Z*	*Y*	6.25	2.35	1.05
3	25.26	12.68	12.65	31.95	274.2	83.0	*Y–Z*	*Y*	2.68	2.35	1.05
4	25.36	12.65	12.67	32.04	272.6	83.0	*X–Y*	*X*	5.55	2.35	1.05
5	25.25	12.65	12.67	31.94	273.2	83.0	*X–Y*	*X*	3.08	2.35	1.05
6	25.21	12.65	12.68	31.90	274.2	82.9	*X–Y*	*X*	1.51	2.35	1.05
7	25.30	12.68	12.65				*Y–Z*	*Y*	10.30	0.71	1.00
8	24.88	12.68	12.65				*Y–Z*	*Y*	6.58	1.20	1.00
9	25.34	12.64	12.68				*Y–Z*	*Y*	11.15	2.00	1.00
10	25.22	12.65	12.68				*X–Y*	*X*	5.30	0.67	0.90
11	25.30	12.65	12.68				*X–Y*	*X*	4.72	0.87	0.90
12	25.48	12.65	12.67				*X–Y*	*X*	5.53	1.35	0.90

X and *Y* axes are shown in Fig. 2. The cut location plane indicates the plane of the cut, and the axis is the axis parallel to the cut. The distance from axis is the distance between the edge of the specimen and the centerline of the notch

the specimens (Fig. 3), and to the *X*, *Y*, and *Z* axes in SolidWorks/CosmosWorks FEA software.

Results and discussion

Determination of elastic constants by RUS

The first 40 resonant frequencies of all the specimens were determined experimentally using RUS before cutting the notches to determine elastic constants of the 4140 steel. Test results were fitted to obtain elastic constants, namely Young's modulus (E) and Poisson's ratio (υ) of the material using Galaxy RPModel software. The average RMS error between measured and calculated resonant frequencies using Galaxy RPModel for the first 40 modes was 0.16%. The average values and standard deviations of c_{11} and c_{44} for the six examined 4140 steel samples were found to be 273.6 ± 0.63 and 83.0 ± 0.06 GPa, respectively, Table 1. These values are in good agreement with the published data. In addition, Table 1 contains positions, widths, and depths of the notches that were cut in 12 different samples.

Numerical and experimental determination of resonant frequencies of undamaged samples

A finite element model of each specimen was constructed using the measured dimensions of the specimens and the calculated elastic constants, and a frequency analysis was performed to determine the resonant frequency spectra. Results of the FEM frequency analysis for the specimens before the cut (without defects) were compared to both the frequency spectrum as determined by RUS and the frequency spectrum as determined by Lagrangian minimization using RPModel software. Resonant frequencies of the first seven modes (out of the 40 modes studied in this work) for Specimen 1 are listed in Table 2, together with the error between resonant frequencies determined using different methods. The average magnitude of the error between any two methods was about 0.3% with a standard deviation of $\pm 0.2\%$.

Numerical and experimental determination of resonant frequencies of samples with defects

The FEM was further modified to determine the variation of modal frequencies as a function of notch depth and location. A total of six cut locations were modeled, three on each face of the specimen, as shown in Fig. 1 and Table 1. The notch depth varied at each location from 0.1 to 2.3 mm (corresponding to about 1–20% of specimen thickness). This resulted in 140 different finite element models with different notch locations and depths. Resonant frequencies from the finite element modes were compared to twelve steel specimens with notches identical to those in the finite element models (Specimens 1–12 in Table 1). Table 2 lists frequencies of the first seven vibration modes for Specimen 1 that were determined by FEM and measured by RUS after the introduction of the defect. The average error between measured and predicted resonant frequencies (the average of the first 40 modes) was 0.63% with a standard deviation of 0.7%. In no case the difference between measured and predicted resonant frequencies did exceed

Table 2 Results of FEM, Lagrange minimization, and RUS for sample 1, before and after the introduction of the notch

Mode	Before defect						After defect		
	FEM (kHz)	Lagrange (kHz)	RUS (kHz)	RUS/FEM error (%)	RUS/Lagrange error (%)	FEM/Lagrange error (%)	FEM (kHz)	RUS (kHz)	RUS/FEM error (%)
X Torsion 1	58.879	58.921	59.160	0.47	0.40	0.07	56.776	57.254	0.83
Y Bend 1	67.042	67.096	67.204	0.24	0.16	0.08	61.509	62.007	0.80
Z Bend 1	67.110	67.155	67.375	0.39	0.33	0.07	64.897	65.337	0.67
Volume 1	100.850	100.909	100.881	0.03	0.03	0.06	94.130	94.698	0.60
Z Bend 2	112.110	112.214	112.233	0.11	0.02	0.09	104.570	105.762	1.13
Y Bend 2	112.190	112.268	112.676	0.43	0.36	0.07	107.280	107.533	0.24
X Torsion 2	117.230	117.339	117.738	0.43	0.34	0.09	111.790	112.450	0.59
Average for the first 40 modes				0.19	0.16	0.12			0.33

FEM Resonant frequencies calculated using finite element analysis

RUS Resonant frequencies measured using RUS

Lagrange Resonant frequencies calculated using Lagrangian minimization (RPModel)

RUS/FEM Error between FEM and RUS frequencies: $\mathrm{RUS/FEM} = 100^{*}|\mathrm{RUS} - \mathrm{FEM}|/\mathrm{RUS}$

RUS/Lagrange Error between Lagrange and RUS frequencies: $\mathrm{RUS/Lagrange} = 100^{*}|\mathrm{RUS} - \mathrm{Lagrange}|/\mathrm{RUS}$

FEM/Lagrange Error between FEM and Lagrange frequency: $\mathrm{FEM/Lagrange} = 100^{*}|\mathrm{FEM} - \mathrm{Lagrange}|/\mathrm{FEM}$

2%. These results validate the use of FEA to predict resonant frequencies of samples with defects (i.e., notches) and show substantial increase in agreement between FEA models and experimental results when compared to previous studies [10, 17].

For each of the 140 cases with different notch positions and lengths, the resonant frequency spectrum was determined using FEM. Frequency spectra of models that included a notch were compared to the original modal frequencies of the model with no cuts to determine the change in the modal resonant frequency caused by the cut. The frequency shift, Δf was calculated as:

$$\Delta f = 100 \cdot \frac{f_{\mathrm{Cut}} - f_{\mathrm{Original}}}{f_{\mathrm{Original}}}[\%], \quad (1)$$

where f is the resonant frequency.

The change in the frequency associated with each vibration mode was analyzed as a function of the notch depth and location to determine the eventual existence of a pattern. Modes were identified via a visual analysis of the mode shape predicted by nodal eigenvectors. For example, for Specimen 1 (defect parallel to *Y* axis, located approximately in the center of the sample), first seven out of 40 calculated modes and modes shapes are illustrated in Fig. 2. It has to be emphasized that particular vibration modes are referred to by name in Fig. 2 and in the rest of this article. For example, the first bending mode about the *Y* axis will be referred to as *Y* Bend 1 or shortly as *Y*1.

Initially, the frequency shift analysis included more than forty vibration modes. For several reasons, it was determined that the seven lowest-order modes provided the best frequency shifts for further analysis. First, for most cut locations and depths, the first seven modes had relatively large changes in frequencies—greater than 1%—and thus greater error between frequencies than the average error determined by RUS and FEA. While some higher-order modes also showed large changes in frequencies for a particular notch location, few of them showed large changes in frequencies for all cut locations. In addition, higher-order modes were not taken into account since they were difficult to identify in finite element frequency spectra. Many of the higher-order vibration modes had similar mode shapes and resonant frequencies and tended to alter greatly in appearance as the depth of the cut increased. Once the depth of the cut was greater than 1% of specimen thickness, visual inspection was insufficient to identity higher-order vibration modes; unlike in the case of lower-order vibration modes. Finally, the higher-order modes tended to group into clusters within tight frequency ranges. As the cut depth increased, certain modes shifted more than others often causing crossing and re-crossing of the high-order vibration modes on the frequency versus notch depth plot. As a result, it was not possible to match a particular resonant frequency with a particular mode using its relative position in the frequency spectra.

Figures 3 and 4 show the frequency shift, Δf, of the first seven modes for some of the studied FEM cases as a function of the notch depth, where depth is expressed as a percentage of specimen thickness. Figures 5 and 6, on the other hand, show the frequency shift of the first seven modes for some of the studied FEM cases as a function of the notch location, where notch location is expressed as a

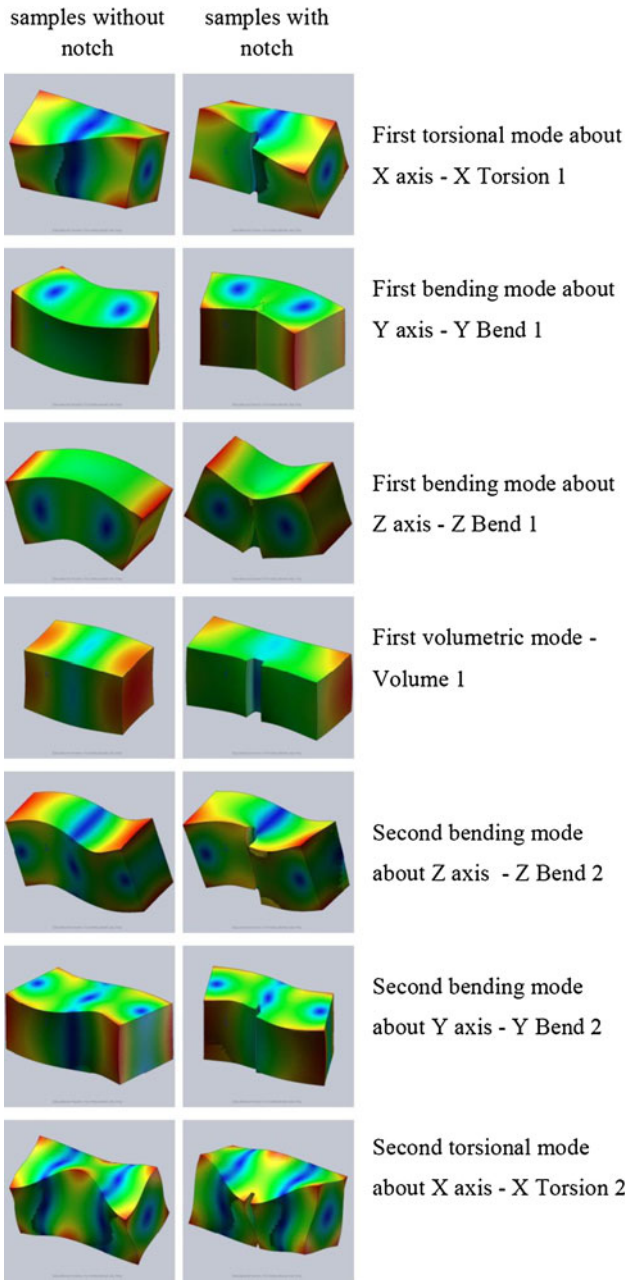

Fig. 2 The first seven vibration modes as determined by FEM for specimen #1 without (*left*) and with (*right*) cut

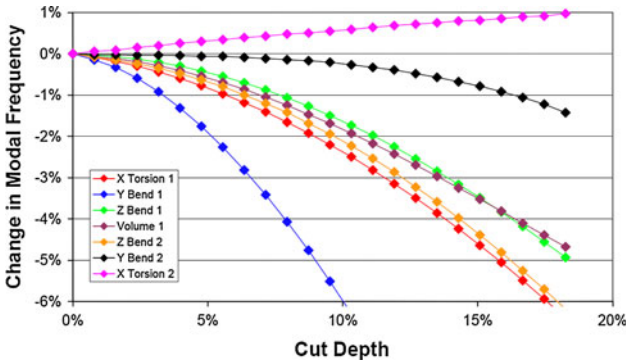

Fig. 3 Change in modal frequency, Δf, versus cut depth for specimen with defect located at 50% and parallel to *Y* axis

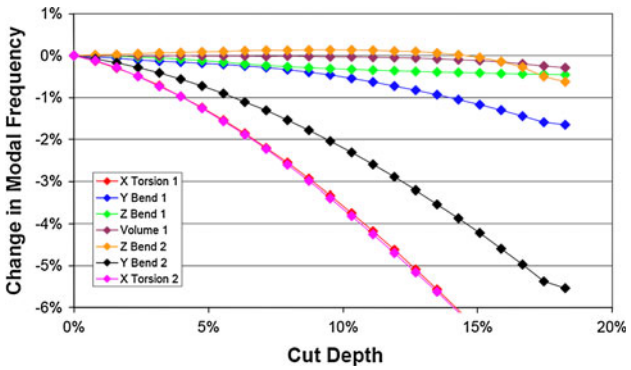

Fig. 4 Change in modal frequency, Δf, versus cut depth for specimen with defect located at 44% and parallel to *X* axis

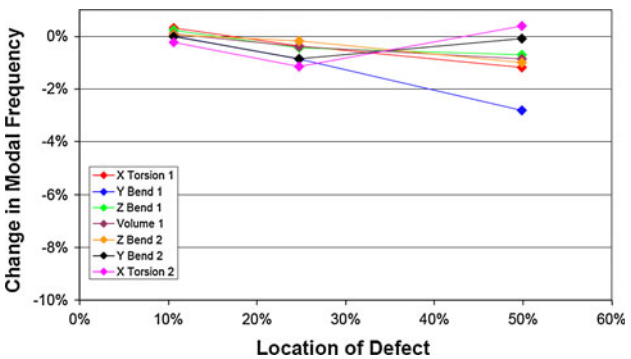

Fig. 5 Change in modal frequency, Δf, versus cut location for specimen with defect of 6% depth and parallel to *Y* axis

percentage of the length of the specimen, measured from one end of the specimen. The change in resonant frequency of each mode is expressed as a percentage of the resonant frequency shift for the sample with defect relative to the sample without the notch, as it is described by Eq. 1.

Defect assessment

As expected, results of both the RUS measurements and the FEA models demonstrate that resonant frequency is affected by the presence of a defect, Figs. 3, 4, 5, 6 and Table 2. Since some modes are more sensitive to certain types of defects, it should be possible to get more information about the size and location of a defect in a specimen by analyzing the change in the resonant frequencies of the specimen. To that end, frequency shift data from the finite element models (not shown here) were analyzed to determine a relationship between the shift in modal resonant frequency and the position and depth of the notch. After

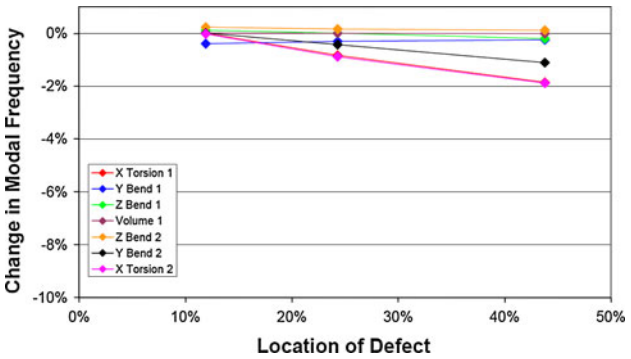

Fig. 6 Change in modal frequency, Δf, versus cut location for specimen with defect of 6% depth and parallel to X axis

testing several different fitting functions, it was found that the following function for a frequency shift of n-th mode provides the best fit:

$$\Delta f_n = C_{0n} + C_{1n}D + C_{2n}DL + C_{3n}DL^2 + C_{4n}D^2 + C_{5n}D^2L + C_{6n}D^2L^2, \quad (2)$$

where D is the depth of the defect expressed as a percent of specimen thickness, and L is the location of the defect expressed as a percent of the specimen length. The change in modal resonant frequency (Δf) is expressed as a percent of the modal resonant frequency of the specimen with no defect, as given by Eq. 1. Higher-order functions of L and D were also tested, but it was found that a second-order function produced results with the lowest average error between measured and predicted values. Regression analyses were performed on the modal frequencies determined by FEA to determine the C_{in} constants from Eq. 2 for the first seven and the first three modes, and the results are shown in Table 3.

A program was created that determined L and D using measured Δf of the sample with the notch for the first seven modes. Essentially, the program assumes values for L and D and then calculates Δf for one or more modes based on the C_{in} constants that were previously determined by linear regression. The program repeats this process iteratively for a large number of L and D values and then chooses the best L and D fits based on a minimum least squares error between the calculated Δf and the actual Δf. If at least two resonant modes are considered in the analysis, the program should converge on a solution of L and D that approximates the value of Δf for both modes. While the C_{in} constants in Eq. 2 are determined using the FEM frequency data for series of samples with different notch depth and location, L and D can be determined from any set of the measured modal frequencies. Therefore, frequencies measured by RUS for the specimens with notches (samples 1–12 in Table 1) were input into the program to estimate L and D for each specimen. Estimates of L and D were compared to actual locations and depths of the notches in the specimens, and the results of this analysis using the first three modes and the first seven resonant modes are presented in Table 4. Calculated positions and depths of the notches for all twelve specimens are presented individually in Table 4, together with the errors between actual and calculated locations and depths of notches using the developed model (Eq. 2).

Table 3 C_{in} constants from Eq. 2 determined by regression analysis

i		X Torsion 1 1	Y Bend 1 2	Z Bend 1 3	Volume 1 4	Z Bend 2 5	Y Bend 2 6	X Torsion 2 7
Defect parallel to Y axis								
0		−0.0001	0.0004	0.0000	−0.0014	−0.0016	−0.0005	0.0001
1	D	0.1156	−0.0525	0.2010	0.1585	−0.0809	0.5304	0.4647
2	DL	−0.4427	0.8397	−1.3433	0.1450	2.1488	−4.0803	−4.3511
3	DL^2	0.0291	−2.4471	1.7720	−1.1321	−4.0829	6.1974	7.1071
4	D^2	0.4995	1.8767	−0.5560	−0.0993	1.6625	−3.9127	−2.9982
5	D^2L	−8.2134	−22.4447	−0.1125	−16.1471	−28.6781	18.6853	14.7971
6	D^2L^2	8.8257	23.1135	−2.9632	28.1882	43.9760	−24.1047	−17.8407
Defect parallel to X axis								
0		0.0006	−0.0002	0.0002	−0.0002	−0.0005	−0.0004	−0.0004
1	D	0.1322	−0.0814	0.0281	0.0117	0.0698	0.1212	0.3647
2	DL	−0.8313	0.2530	−0.0305	−0.0260	−0.1874	−0.3202	−1.7777
3	DL^2	0.0624	−0.1729	−0.2771	0.0671	0.4170	−0.4080	1.0408
4	D^2	0.0958	0.0028	0.0917	−0.0595	−0.1569	−0.4979	−2.4870
5	D^2L	−7.6890	−0.2735	−1.9504	0.0867	0.7157	−4.3141	2.1964
6	D^2L^2	9.5363	−1.9055	4.3070	−0.6275	−3.3941	6.2430	0.4288

Table 4 Errors in predicted position (L) and depth (D) for the first three and seven modes

Actual (%)		Predicted using first seven modes (%)				Predicted using Fust 3 modes (%)			
Depth	Location	Depth	Location	Error		Depth	Location	Error	
				Depth	Location			Depth	Location
Cut parallel to Y axis									
18.6	50	18.1	50.0	0.5	0.1	18.3	49.0	0.2	0.9
18.6	25	18.5	25.0	0.0	0.2	18.8	245	0.2	0.3
18.6	11	19.6	10.5	1.0	0.1	19.6	105	1.0	0.1
5.6	41	5.4	45.0	0.2	4.3	5.8	43.0	0.2	2.3
9.5	26	92	28.5	0.3	2.1	10.0	26.0	0.5	0.4
15.8	44	15.4	48.5	0.4	4.5	15.4	47.5	0.4	3.5
Average error (FEM)				0.4	1.5			0.4	1.3
Average error (actual)				0.4	1.9			0.4	1.2
Cut parallel to X axis									
18.6	44	17.1	51.0	1.5	7.2	22.5	255	39	18.3
18.6	24	18.1	235	0.4	0.8	17.5	25.0	1.1	0.7
18.6	12	25.0	13.0	6.4	1.1	25.0	10.0	6.4	1.9
5.3	42	4.8	34.0	0.5	7.8	5.6	29.0	0.3	12.8
6.9	37	63	35.5	0.6	1.7	6.7	32.5	0.2	4.7
10.7	44	11.5	33.5	0.8	10.1	12.5	295	1.8	14.1
Average error (FEM)				0.3	1.8			0.1	1.5
Average error (actual)				1.7	4.8			23	9.9

Final remarks

A high degree of agreement can be achieved between actual and estimated locations (L) and depths (D), as shown in Table 4. Main sources of error include errors in specimen dimensions, particularly in the notch depth and location. The notches were modeled as perfectly straight and parallel to the axis of the steel bar. However, in reality, cuts were slightly angled relative to the axis and were wider at the top than the bottom. Other sources of error include internal damping of the specimen. The later is most likely not a significant source of error in this case since FEA predicted frequencies are within 1% of actual measurements.

The lower-order modes are typically the most sensitive to the notch depth—particularly the first Y bending mode (Y Bend 1) when the notch is parallel to the Y axis and the first X torsional mode (X Torsion 1) when the notch is parallel to the X axis. This is to be expected since those modes are most affected by changes in stiffness along those axes. The reduction in specimen thickness can be expressed as a reduction in specimen stiffness. In fact, previous studies have attempted to use stiffness as a predictor of crack depth with some success [10]. Higher-order modes are sensitive to cut depth but typically have some "threshold depth value." At cut depths less than the threshold value, there is very little change in modal frequency. This is particularly noticeable when the cut is near the edge of the specimen.

It should be noted that as the cut length increases, the frequency shift will approach 100% in all cases regardless of location. The approximation used in this analysis [$\Delta f = f(D,\ D^2,\ L,\ L^2)$] should only be used for certain values of depth. Therefore, part of any prediction of depth and location must include an analysis of the FEA output to determine the order of the best-fit function.

Conclusions

In this study, RUS, in combination with FEA, was used to determine the size and location of a defect in a specimen of known geometry and elastic constants. Analyses of FEA resonant frequency spectra can be used to determine acceptable criteria for the frequency spectrum of an object with a simple geometry without the requirement of testing a large number of undamaged and damaged objects. In addition, it is possible to determine not only if an object has a defect but also the location and size of the defect by analyzing the frequency spectrum. Analyses of the steel specimens with 1 mm wide cuts demonstrate that FEA estimates of resonant frequencies are quite close to measured resonant frequencies. Therefore, FEA results can be used to predict behavior of actual objects with or without

defects. By analyzing predicted resonant frequencies of many different FEA models, certain trends in the behavior of particular resonant modes became evident. When measured resonant frequencies of specimens with defects of arbitrary location and depth were analyzed using the method outlined in this paper, these trends in the FEA data could be used to determine the defect location with an average error less than 5% of the specimen length and the defect depth with an average error of less than 2% of the specimen thickness. These results demonstrate the practicability of using FEA to determine acceptance/rejection criteria for NDT in the case of small samples with simple geometries.

Acknowledgements Authors would like to thank Texas Engineering Experimental Station for financial support and Prof. Arroyave, Prof. Kinra, and Prof. Benner from Texas A&M University for precious suggestions and comments.

References

1. Shull PJ (2002) Nondestructive evaluation: theory, techniques, and applications. Marcel Dekker, New York
2. Hellier C (2003) Handbook of non-destructive evaluation. McGraw-Hill, New York
3. Bray DE, Stanley RK (1997) Nondestructive evaluation: a tool in design, manufacturing, and service. CRC Press, Boca Raton
4. Migliori A, Sarrao JL (1997) Resonant ultrasound spectroscopy: applications to physics, materials measurements, and nondestructive evaluation. Wiley, New York
5. De Silva CW (2000) Vibration: fundamentals and practice. CRC Press, Boca Raton
6. Ulrich TJ (2000), MS Thesis, Department of Physics, University of Nevada Reno
7. Vuorinen JF, Schwarz RB (2000) J Alloys Comp 310:7
8. Kam TY, Lee TY (1992) Eng Fract Mech 42:381
9. Lee YS, Chung MJ (2000) Comput Struct 77:327
10. Rizos PF, Aspragathos N, Dimarogonas AD (1990) J Sound Vib 138:381
11. Kaewunruen S, Remennikov AM (2007) NDT & E Int 40:510
12. Erauw JP, VanderGucht A, Cambier F (2004) Euro Ceram 8: 264
13. Gheorghiu C, Rhazi JE, Labossiere P (2005) Can J Civil Eng 32:1093
14. Cawley P, Adams RD (1979) J Strain Anal Eng Des 14:49
15. Radovic M, Lara-Curzio E, Riester L (2004) Mat Sci Eng A 368:56
16. Leisure RG, Willis FA (1997) J Phys Condens Matter 9:6001
17. Belyaev A, Polupan O, Ostapenko S, Hess D, Kalejs JP (2006) Semicond Sci Technol 21:254
18. Dallas W, Polupan O, Ostapenko S (2007) Meas Sci Technol 18:852
19. Zadler BJ, Le Rousseau JHL, Scales JA, Smith ML (2004) Geophys J Int 156:154
20. Thomson WT (1972) Theory of vibration with applications. Prentice-Hall, Englewood Cliffs
21. Fertis DG (1995) Mechanical and structural vibrations. Wiley, New York
22. Visscher WM, Migliori A, Bell TM, Reinert RA (1991) J Acoust Soc Am 90:2154
23. Stekel A, Sarrao J, Bell T, Lei M, Leisure R (1992) J Acoust Soc Am 92:663
24. Gupta KK, Meek JL (2000) Finite element multidisciplinary analysis. American Institute of Aeronautics and Astronautics, Reston
25. Reddy JN (2006) An introduction to the finite element method, 3rd edn. McGraw-Hill Higher Education, New York
26. Ross CTF (1098) Advanced finite element methods. Horwood, Chichester